CHALMERS
UNIVERSITY OF TECHNOLOGY

Effect of engine dynamics on optimal power-split control strategies in hybrid electric vehicles

Effect of Engine Dynamics on Optimal Power-Split Control Strategies in Hybrid Electric Vehicles

Anand Ganesan[*,1,3] Sébastien Gros[2] Nikolce Murgovski[3] Chih Feng Lee[1] Martin Sivertsson[1]

***Abstract*—This paper presents a model predictive control (MPC) based supervisory power-split control strategy, which optimises fuel and energy consumption in Hybrid Electric Vehicles (HEVs) by incorporating powertrain actuator dynamic models. In HEVs, while distributing the driver demand to the powertrain actuators, a standard approach is to approximate the actuator energy conversion dynamics with steady-state maps, which leads to sub-optimal control policy and increased fuel & energy consumption, especially for a driving mission with high transient demands. To address this shortfall, the control strategy proposed in this paper explicitly integrates an experimentally validated dynamic model of gasoline internal combustion engine (ICE) into an MPC based power-split controller. The proposed strategy is validated in a parallel HEV platform, where the sensitivity of the HEV energy consumption w.r.t. its actuator dynamics and the transients in its load demands, is also established. The results enable an understanding of the energy saving potential in HEVs that supports the inclusion of actuator dynamic models in optimal power-split controllers and it also establishes that the proposed control strategy realises higher energy and fuel savings in HEVs.**

***Index Terms*—Engine Dynamics, Powertrain Actuator Dynamics, Fuel consumption, Optimal Energy Management, Dynamic Optimisation, MPC, parallel Hybrid, HEV, Optimal Strategies, power-split, torque-split.**

I. Introduction

In the field of powertrain control, supervisory control strategies for hybrid electric vehicles (HEVs) have been a very active research field [1]–[7], as the electrification of mobility platforms is growing exponentially [8]. A typical HEV is an over-actuated system i.e., its powertrain consists of an internal combustion engine (ICE) and one (or) more electrical machines (EM), as its actuators [9]. A key control challenge in a HEV is to allocate its total propulsive/braking demand to its actuators such that either the total fuel consumption or the energy consumption is optimised for a driving mission [2], [3], [9]. To address this problem, several control strategies have been proposed so far, such as 1) deterministic or rule-based strategies [10], [11] and fuzzy-logic based control strategies [12]–[14], which rely on empirical relationships and/or pattern recognition, 2) Equivalent consumption minimisation strategies (ECMS), which rely on minimising a Hamiltonian function at each time step to find a local optima [3]–[5], [9], [15]–[17] and 3) Dynamic programming based strategies, which find the global optima but are computationally intensive, since they perform brute-force search of the entire state-space of feasible solutions [9], [11], [18].

Among these strategies, a standard approach to model the energy conversion dynamics of the powertrain actuators is to approximate them as steady state efficiency maps for control allocation [1]–[7], [9], [16], [17]. Under high transient load demands (a typical use case in HEV's), this method creates mismatch between plant output and controller prediction as it ignores 1) the actuator dynamics and 2) the potential cost for transition between two operating points, hence resulting in a sub-optimal control policy leading to increased fuel and energy consumption [19]–[21]. Fewer studies have shown the possibility of fuel and energy savings by using additional static correction/penalty parameters (derived from the dynamic plant models, like start-up transient consumption, airflow and fuel-torque conversion models, of a diesel engine in [19] and from the ICE and clutch dynamic models of a gasoline engine in [21]) in the control objective of torque-split controllers to minimise transient consumption. This is an approximate way of incorporating the effects of powertrain dynamics in HEV torque split strategies.

In this paper we further the above understanding by 1) proposing a detailed dynamic model of gasoline ICE that accounts for both slower dynamics governed by air mass flow dynamics, fuel flow dynamics, kinetic energy in engine's crankshaft and flywheel [22], [23] and relatively faster dynamics led by combustion efficiency control and emission control, 2) explicitly incorporating powertrain actuator dynamic models (ICE in this study) as 'states' within the power-split controller formulated using MPC, which enables the controller to predict the trajectory of dynamics accurately and 3) analysing the sensitivity of the energy saving potential in a HEV w.r.t. the actuator (ICE) dynamic model parameter variations and the driving mission's transient load demand variations.

II. Control-Oriented Modelling of Parallel HEV Powertrain Dynamics

In this section, control-oriented dynamic models of different components/systems in a parallel HEV powertrain configuration considered for this study (see Fig. 1), are described. The considered powertrain includes an internal combustion engine (ICE), an integrated starter generator (ISG), a 8-speed

The research work has been performed with support from the *Sweden´s Innovation Agency (Vinnova)*.

[*] Corresponding author. Email: anand.ganesan@volvocars.com.
[1] *Vehicle Software and Electronics, Volvo Car Corporation*, Göteborg, Sweden. Email: chih.feng.lee@volvocars.com; martin.sivertsson@volvocars.com.
[2] *Department of Engineering Cybernetics, Norwegian University of Science and Technology*, Trondheim, Norway. Email: sebastien.gros@ntnu.no.
[3] *Department of Electrical Engineering, Chalmers University of Technology*, Göteborg, Sweden. Email: nikolce.murgovski@chalmers.se.

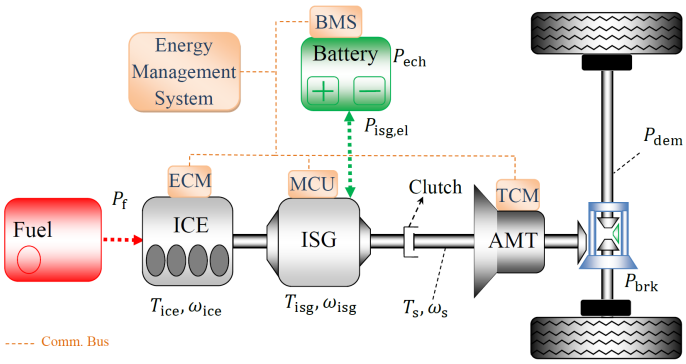

Fig. 1. Parallel HEV powertrain configuration.

auto-transmission unit, a battery, a differential along with other driveline components, wheels, and respective low-level controllers of all these components, see Fig. 1.

A. Vehicle Dynamics

Using point mass representation, the longitudinal vehicle dynamics can be modelled as [4], [9]:

$$\dot{s}(t) = v(t), \tag{1a}$$

$$\dot{v}(t) m_{\mathrm{e}}(\cdot) = F(t) + F_{\mathrm{brk}}(t) - \frac{c_{\mathrm{a}} v^2(t)}{2} - mg\left(\sin\alpha(s) + c_{\mathrm{r}}\cos\alpha(s)\right), \tag{1b}$$

where $c_{\mathrm{a}} = c_{\mathrm{d}} A_{\mathrm{f}} \rho_{\mathrm{air}}$, c_{d} is the aerodynamic drag coefficient, A_{f} is the vehicle frontal surface area, ρ_{air} is the air density, s is the travelled distance, m is the vehicle mass, α is the road slope, c_{r} is the rolling resistance coefficient, F is the traction force from the ICE and the ISG, F_{brk} is the force dissipated within the friction brakes, v is the linear velocity of the vehicle and m_{e} is the equivalent mass computed as [5], [24]:

$$m_{\mathrm{e}}(\cdot) = m + \frac{J_{\mathrm{wh1}} + x_{\mathrm{clt}}(t)(J_{\mathrm{ice}} + J_{\mathrm{isg}})(R_\gamma(\gamma) R_{\mathrm{dg}})^2}{r_{\mathrm{wh1}}^2}, \tag{2}$$

where x_{clt} is the transmission clutch engagement status, R_γ is the ratio of chosen gear γ, R_{dg} is the fixed ratio of the differential gear, r_{whl} is the wheel radius, J_{whl} is the rotational inertia of all the powertrain components (except ICE and ISG) reflected at the wheels, J_{ice} and J_{isg} are the inertia of the ICE and the ISG, respectively. If the trajectories of $v(t), \alpha(t)$ are known a priori, then using (1) and assuming that the brake controller always ensures $F_{\mathrm{brk}}(t) = 0$ when $F(t) \geq 0$ and $F_{\mathrm{brk}}(t) \in \mathbb{R}^-$, the power demand trajectory at the wheels can be pre-calculated for $\forall t$ as:

$$P_{\mathrm{dem}}(t) = \begin{cases} F(t)v(t), & F(t) \geq 0, \\ \left(F(t) + F_{\mathrm{brk}}(t)\right) v(t), & F(t) < 0. \end{cases} \tag{3}$$

B. Transmission and Drivetrain Components

Assuming the clutch lock-up i.e. $x_{\mathrm{clt}}(t) = 1$, $\forall t$, auto-transmission (controlled by transmission control module, TCM) and drivetrain components (differential, axle shafts and joints) can be modelled as [5]:

$$P_{\mathrm{isg}}(t) + P_{\mathrm{ice}}(t) = \begin{cases} P_{\mathrm{dem}}(t)/\eta_\gamma(\gamma), & P_{\mathrm{dem}}(t) \geq 0 \\ P_{\mathrm{dem}}(t)\eta_\gamma(\gamma), & P_{\mathrm{dem}}(t) < 0 \end{cases} \tag{4}$$

$$\gamma(t) \in \{0, 1, 2, .., \gamma_{\max}\}, \tag{5}$$

where $\eta_\gamma(\gamma)$ is the net efficiency of the chosen gear γ and differential gear, P_{isg} is the ISG power and P_{ice} is the power delivered by the ICE. The TCM uses a map-based gear shifting algorithm to decide the suitable gear $\gamma(t)$ based on the velocity, $v(t)$ & power demand, $P_{\mathrm{dem}}(t)$.

C. Internal Combustion Engine (ICE) Dynamics

A supercharged gasoline internal combustion engine with an integrated Engine Control Module (ECM) is considered in this work. ECM ensures that the ICE delivers the requested power provided that the request is within bounds, as in:

$$P_{\mathrm{ice,min}}(\omega_{\mathrm{ice}}) \leq P_{\mathrm{ice,req}}(t) \leq P_{\mathrm{ice,max}}(\omega_{\mathrm{ice}}). \tag{6}$$

ICE angular velocity, ω_{ice} is given by eqs. (7) and (8), where $\omega_{\mathrm{ice,min}}$ refers to the idling speed of the engine [5]:

$$\omega_{\mathrm{ice}}(t) = \begin{cases} \omega_{\mathrm{ice,min}}, & \gamma(t) = 0, \\ v(t) R_\gamma(\gamma) R_{\mathrm{dg}} / r_{\mathrm{whl}}, & \gamma(t) \geq 1, \end{cases} \tag{7}$$

$$\omega_{\mathrm{ice}}(t) \in [\omega_{\mathrm{ice,min}}, \omega_{\mathrm{ice,max}}]. \tag{8}$$

D. Integrated Starter Generator (ISG) and Battery Model

The ISG is represented by a Quasi-static model, as in [5]:

$$P_{\mathrm{isg,el}}(t) = P_{\mathrm{isg}}(t) + P_{\mathrm{isg,ls}}\left(\omega_{\mathrm{isg}}(t), P_{\mathrm{isg}}(t)\right), \tag{9}$$

$$\omega_{\mathrm{isg}} = \omega_{\mathrm{ice}}, \tag{10}$$

$$P_{\mathrm{isg}}(t) \in [P_{\mathrm{isg,min}}(\omega_{\mathrm{isg}}), P_{\mathrm{isg,max}}(\omega_{\mathrm{isg}})], \tag{11}$$

where $P_{\mathrm{isg,ls}}$ is the static map of the ISG powerloss, ω_{isg} and P_{isg} are the angular speed and the mechanical power of the ISG, respectively. The battery dynamics is represented using a simplified model, as in:

$$\dot{x}_{\mathrm{b}}(t) = -P_{\mathrm{ech}}(\cdot)/E_{\mathrm{b,max}}, \tag{12}$$

$$x_{\mathrm{b}}(t) \in [\ 0 \leq x_{\mathrm{b,min}}\ ,\ x_{\mathrm{b,max}} \leq 1\ ], \tag{13}$$

where x_{b} is the state of energy (SOE), $E_{\mathrm{b,max}}$ is the energy capacity, and P_{ech} is the rate of consumption of stored electro-chemical energy which can be computed as:

$$P_{\mathrm{ech}}(t) = P_{\mathrm{isg,el}}(\omega_{\mathrm{isg}}(t), P_{\mathrm{isg}}(t)) + P_{\mathrm{aux}}(t) + R_{\mathrm{b}}(x_{\mathrm{b}}(t)) P_{\mathrm{ech}}^2(\cdot)/U_{\mathrm{ocv}}^2(x_{\mathrm{b}}(t)), \tag{14}$$

where P_{aux} is the auxiliary power, R_{bat} and U_{ocv} are the lumped internal resistance and the open circuit voltage of the battery, respectively. The algebraic solution for (14) is [17]:

$$P_{\mathrm{ech}}(t) = \frac{U_{\mathrm{ocv}}^2(x_{\mathrm{b}})}{2R_{\mathrm{b}}(x_{\mathrm{b}})} - U_{\mathrm{ocv}}(x_{\mathrm{b}}) \frac{\sqrt{U_{\mathrm{ocv}}^2(x_{\mathrm{b}}) - 4R_{\mathrm{b}}(x_{\mathrm{b}}) P_{\mathrm{isg,el}}(t)}}{2R_{\mathrm{b}}(x_{\mathrm{b}})}. \tag{15}$$

III. Modelling Gasoline ICE Dynamics

Modelling the dynamics of the ICE accurately is quite challenging due to the highly complex nonlinear interactions of its sub-systems. But, the input-output dynamics of the system considered here i.e., an ICE with an integrated ECM (with torque compensation mechanisms to deliver the requested performance), becomes simpler and predictable due to its closed-loop nature [19], [22]. Hence, in this section we propose dynamic models for such an actuator-controller closed-loop system that can effectively map both its transient and steady-state behaviours w.r.t. fuel consumption and torque production, which are two key parameters affecting both the control strategy and the total energy consumption in a HEV.

A. Dynamic Torque Model

Among the major factors that affect the gasoline ICE torque dynamics, the control of the air-mass flow dynamics in the intake and exhaust manifolds, the fuel flow dynamics in intake, and the kinetic energy in the engine's crankshaft and flywheel typically exhibit slower response when compared to the faster torque response provided by the combustion efficiency (η_{i}) control achieved using the ignition retard/advance [19], [20], [22]. A simplified first-order transient torque model that captures the dynamics of the slow response factors in a diesel engine was proposed in [19] as:

$$\tau_{\mathrm{ice}}(\dot{T}_{\mathrm{ice,req}})\ \dot{T}_{\mathrm{ice}}(t) + T_{\mathrm{ice}}(t) = T_{\mathrm{ice,req}}(t), \tag{16}$$

where, $T_{\mathrm{ice,req}}$ and T_{ice} are the request and the output torques, respectively, the ICE time constant (τ_{ice}) is piece-wise affine on the rate of change of the request $\dot{T}_{ice,req}$ as in [19]:

$$\tau_{ice} = \begin{cases} \tau_1, & \dot{T}_{ice,req} \geq 0, \\ \tau_2, & \dot{T}_{ice,req} < 0. \end{cases} \tag{17}$$

Since, all the slow response factors have similar effects in a gasoline engine and the fact that the control of η_{i} (used to achieve different performance criterion including suppression of drivetrain torque oscillations, knock protection and smooth acceleration) is an additional degree-of-freedom in a gasoline engine control [22], [23], the model in (16) can be modified to estimate the dynamic torque of the gasoline ICE as follows:

$$\tau_{\mathrm{ice}}(\dot{T}_{\mathrm{ice,req}})\ \dot{T}_{\mathrm{ice}}(t) + T_{\mathrm{ice}}(t) = \eta_{\mathrm{i}}(t)\frac{P_{\mathrm{ice,req}}(t)}{\omega_{\mathrm{ice}}(t)}, \tag{18}$$

$$T_{\mathrm{ice}}(t) \in [T_{\mathrm{ice,min}}(\omega_{\mathrm{ice}}), T_{\mathrm{ice,max}}(\omega_{\mathrm{ice}})]. \tag{19}$$

B. Dynamic Fuel Consumption Model

The rate of energy consumption of the ICE, from gasoline fuel under steady state operation, can be represented as $P_{\mathrm{f,ss}}(\omega_{\mathrm{ice,ss}}, T_{\mathrm{ice,ss}})$ in watts, where $\omega_{\mathrm{ice,ss}}$ and $T_{\mathrm{ice,ss}}$ are the steady-state angular speed and torque, respectively. The dynamic energy consumption rate $P_{\mathrm{f}}(t)$ can then be estimated using $P_{\mathrm{f,ss}}$, the dynamic torque from (18), stoichiometric ratio λ_{f}, and the ignition efficiency η_{i}, as in:

$$P_{\mathrm{f}}(t) = \frac{P_{\mathrm{f,ss}}\left(\omega_{\mathrm{ice}}(t), T_{\mathrm{ice}}(t)/\eta_{\mathrm{i}}(t)\right)}{\lambda_{\mathrm{f}}(t)}, \qquad \lambda_{\mathrm{f}}(t) \in [\lambda_{\mathrm{f,min}}, \lambda_{\mathrm{f,max}}]. \tag{20}$$

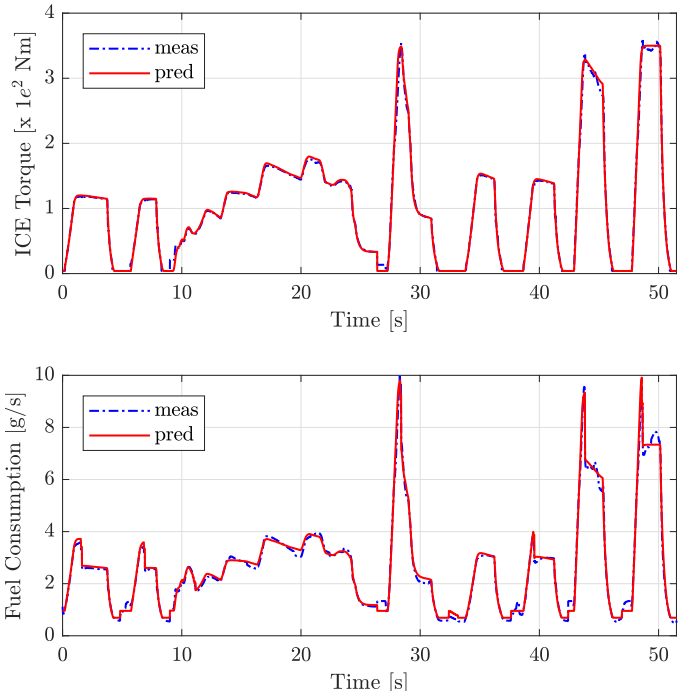

Fig. 2. Validation results of the proposed dynamic models for prediction of torque and fuel consumption of the ICE. The models exhibit a mean absolute percentage error (MAPE) of 2.5% and 3.8%, respectively within the operating speed range of interest (1000rpm $\leq \omega_{\mathrm{ice}} \leq$ 4000rpm). Blue dash-dotted line indicates the measurements and the red solid line shows the prediction.

C. Experimental Validation of Dynamic Models

The dynamic models proposed in III-A and III-B were validated experimentally for both steady-state and transient operating points, i.e. ω_{ice} and T_{ice}. Figure 2, shows the comparison between the dynamic model prediction and the measurements for both torque developed and fuel consumption, respectively. Our results show that the dynamic torque model prediction has a mean absolute percentage error (MAPE) of 2.5% between 1000rpm - 4000rpm and 10% above 6000rpm. Similarly, the fuel consumption estimate (converted to g/s for representation) of the dynamic model has an MAPE of 3.8% between 1000rpm - 4000rpm and 13.3% above 6000rpm. These results show that the prediction accuracy of the proposed dynamic models are suitable for the considered HEV power-split supervisory control. The inclusion of η_{i} in (20), is to consider the additional fuel consumed by the torque compensation mechanisms specified earlier in section III-A.

IV. Optimal Power-Split Strategy using MPC Formulation

In this section, a supervisory optimal power-split control strategy for a parallel HEV is proposed, in which the dynamic models of the powertrain actuator (ICE) are explicitly included as dynamic 'state' constraints in the optimal controller. The proposed strategy is implemented using MPC to validate it and to study the sensitivity of the total energy consumption w.r.t. variations in τ_{ice} (18), in the HEV platform.

A. Supervisory Power-Split Strategy

We consider a problem where an oracle (higher-level controller) predicts the trajectories of vehicle speed $v(t)$, road slope $\alpha(t)$, battery co-state $\lambda_{\mathrm{b}}(x_{\mathrm{b}}(t))$ and the integer decisions like clutch on-off $x_{\mathrm{cl}}(t)$ and gear $\gamma(t)$ for a given mission. Then, $\omega_{\mathrm{ice}}(t)$ and $\omega_{\mathrm{isg}}(t)$ are known from eqs. (7) and (10) and the power demand $P_{\mathrm{dem}}(t)$ w.r.t. the engine speed $\omega_{\mathrm{ice}}(t)$ for $\forall t$ can be calculated from eqs. (1) to (4). Now, the objective of the power-split controller is to find a control input $u(t)$, that allocates the demand to the powertrain actuators while minimising the overall energy consumption of the HEV over a specific horizon, $t \in [t_0, t_{\mathrm{f}}]$. Hence, the cost function can be stated as [3], [16], [17]:

$$J(\cdot) = \int_{t_0}^{t_{\mathrm{f}}} \left(P_{\mathrm{f}}(x(t), u(t), d(t)) + \lambda_{\mathrm{b}}(x_{\mathrm{b}}(t)) P_{\mathrm{ech}}(x(t), u(t), d(t))\right) dt, \tag{21}$$

where the first and second terms refer to the fuel consumption and the battery energy, respectively, $x(t)$ refers to the state dynamics of the ICE torque, $u(t)$ and $d(t)$ are control input and disturbances, respectively, $\lambda_{\mathrm{b}}(x_{\mathrm{b}}(t))$ is the SOE-dependent battery co-state (equivalence factor) that relates the battery energy cost to the fuel consumption, which the oracle optimises in real-time and shares the λ_{b}^{*} trajectory to the power-split controller (refer [3], [17], [20] to know about the co-state optimisation in HEVs). Further, the variation of the internal battery parameters, $U_{\mathrm{ocv}}(t)$ and $R_{\mathrm{b}}(t)$, are negligible for small deviations of the SOE in a parallel HEV and hence it is reasonable to neglect the SOE dependence in (15) [3]. So, $U_{\mathrm{ocv}}(t)$, $R_{\mathrm{b}}(t)$ and $\lambda_{\mathrm{b}}(t)$ (assuming SOE bounds are not active) would remain approximately constant for an MPC update but follows the oracle's mission trajectory across the updates. Under these assumptions, it is possible to pre-compute the braking force $F_{\mathrm{brk}}^{*}(t)$ for $\forall t$ by saturating the requested power to the ISG bound $P_{\mathrm{isg,min}}(\omega_{\mathrm{isg}}(t))$, thereby simplifying the mechanical power balance (4) to:

$$P_{\mathrm{isg}}(t) = P_{\mathrm{dem}}(t) - P_{\mathrm{ice}}(t). \tag{22}$$

B. MPC Formulation

MPC is used to implement the proposed strategy since it is an effective optimal control tool that optimises a cost function subject to constraints over a prediction horizon [1]–[4], [19], [21]. The proposed strategy can be represented as follows:

$$\min_{u} \int_{\tau}^{\tau+t_{\mathrm{h}}} J\left(x(t|\tau), u(t|\tau), d(t|\tau)\right)\ dt \tag{23a}$$

$$\text{s.t.} \quad \dot{x}(t|\tau) = (u(t|\tau) - x(t|\tau))/\tau_{\mathrm{ice}}, \tag{23b}$$

$$u_{\min}(d(t|\tau)) \le u(t|\tau) \le u_{\max}(d(t|\tau)), \tag{23c}$$

$$x_{\min}(d(t|\tau)) \le x(t|\tau) \le x_{\max}(d(t|\tau)), \tag{23d}$$

$$x(\tau|\tau) = x_0(\tau), \tag{23e}$$

where the state (dynamics), the control input, disturbances and the cost are:

$$x(t|\tau) = T_{\mathrm{ice}}(t|\tau), \qquad u(t|\tau) = P_{\mathrm{ice,req}}(t|\tau), \tag{24a}$$

$$d(t|\tau) = \begin{bmatrix} \omega_{\mathrm{ice}}(t|\tau) & \omega_{\mathrm{isg}}(t|\tau) & x_{\mathrm{b}}(\tau) & \lambda_{\mathrm{b}}(\tau) \\ & \lambda_{\mathrm{f}}(t|\tau) & \eta_{\mathrm{i}}(t|\tau) & P_{\mathrm{dem}}(t|\tau) & P_{\mathrm{aux}}(t|\tau) \end{bmatrix}^{T}, \tag{24b}$$

$$J(\cdot) = P_{\mathrm{f}}(\eta_{\mathrm{i}}, \lambda_{\mathrm{f}}, \omega_{\mathrm{ice}}, T_{\mathrm{ice}}) - \frac{\lambda_{\mathrm{b}} P_{\mathrm{ech}}(x_{\mathrm{b}}, \omega_{\mathrm{isg}}, P_{\mathrm{dem}} - P_{\mathrm{ice}}, P_{\mathrm{aux}})}{E_{\mathrm{b,max}}}. \tag{24c}$$

The problem is solved for $t \in [\tau, \tau + t_{\mathrm{h}}]$ and $\tau \in [t_0, t_{\mathrm{f}} - t_{\mathrm{h}}]$.

V. Simulation and Results

A dynamic simulation of the considered power-split problem (23) was carried out using the plant models of the considered HEV platform, described in II and III.

A. Simulation Strategy

To validate the proposed control strategy, a hybrid approach (refer [25, p. 12] for pictorial representation) was adopted, i.e. a backward simulator is first used to determine the optimal power split using the predicted information (refer section IV-A for details on predicted trajectories). These optimal controls are then applied to the forward simulator plant models and the corresponding state trajectories of the powertrain and vehicle dynamic plants are determined. The forward simulator also uses a feedback mechanism to recover the vehicle speed deviations, due to actuator dynamics mismatch (between the controller and the plant models) and powertrain saturation, and allocates the corresponding additional tractive demand to the actuator set-point. Also, to enable effective analysis of the results, the scenarios and assumptions listed below were used.

- In addition to the simulation of the MPC strategy proposed in (23), referred as dynamic MPC (dy-MPC), a baseline MPC strategy without ICE dynamics, referred to as static-MPC (st-MPC), was also formulated by removing state constraint (23b) from (23) and simulated for comparison.
- Both dy-MPC and st-MPC were discretized with a sampling interval of $t_{\mathrm{s}} = 0.025\,\mathrm{s}$ and a $20\,\mathrm{s}$ time interval was chosen as prediction horizon.

B. Performance Evaluation of the Proposed Strategy

The proposed strategy is evaluated using the WLTC Class-3b cycle, shown in Fig. 3(a), to check the performance under the combined effect of different driving scenarios like Urban, Semi-Urban, Motorway, and Extra High-Speed (i.e., different scenarios are suitably weighted in a single cycle), and the results are shown in Fig. 3(b) and Fig. 4.

1) Actuator Torque Trajectories - Controller Prediction Vs Plant Output : From Fig. 3(b) it could be observed that i) the optimal ICE torque (also referred as 'predicted ICE torque' in this paper) trajectories, i.e., the trajectory of optimal torque allocated to the ICE by both the power-split controllers (top figure in Fig. 3(b)), deviate from each other (for e.g., at time

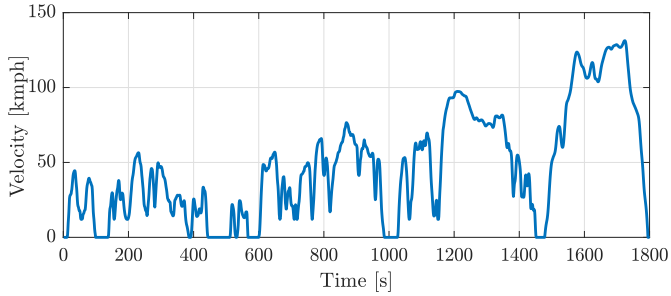

(a) WLTC Class-3b driving cycle used for simulation.

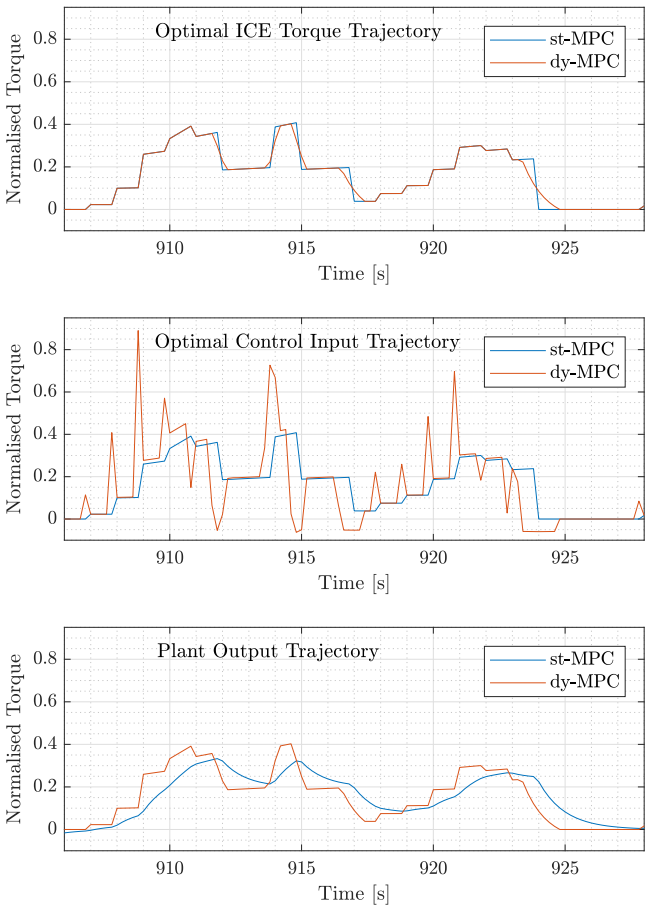

(b) Effect of dynamics ($@\tau_{\text{ice}} = 1\,\text{s}$) on the optimal ICE torque, optimal control input and ICE plant output trajectories. Dy-MPC delivers an optimal control policy whereas st-MPC struggles due to actuator dynamics mismatch.

Fig. 3. Simulation results of proposed optimal power-split control strategy.

instances 912 s, 914 s, 915 s, 917 s, and 924 s) whenever the gradient of dy-MPC's torque trajectory is saturated or limited by the ICE model dynamics and control input saturation, respectively, i.e., due to the inclusion of the state dynamics as an additional constraint in dy-MPC, it's feasible region becomes smaller relative to the feasible region of st-MPC, ii) the optimal control input trajectory of both controllers (centre figure in Fig. 3(b)) show considerable difference between them due to the fact that the dy-MPC optimises its control input to compensate for the ICE dynamics (conversely, input saturation

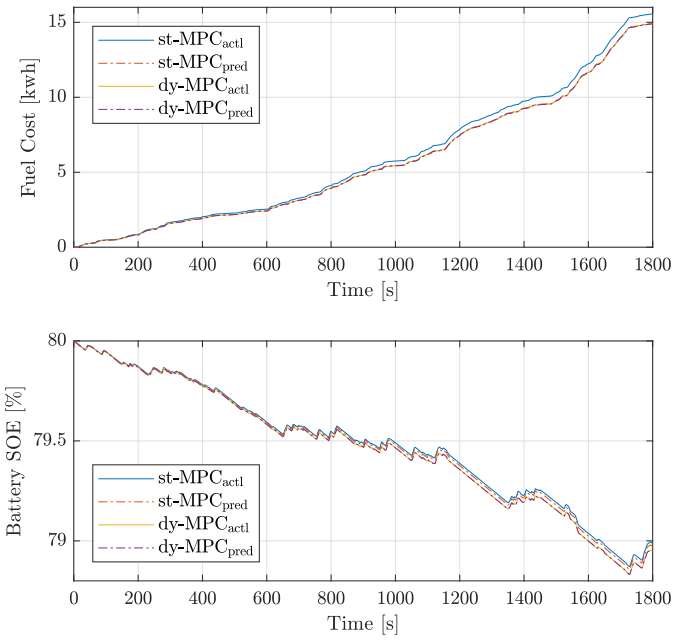

Fig. 4. Predicted and actual trajectories of cumulative fuel (top figure) and battery (bottom figure) energy consumption of both controllers, $@\tau_{\text{ice}} = 1\,\text{s}$. The proposed strategy, dy-MPC, was able to achieve a total energy saving of 4.25% w.r.t. st-MPC.

limits the gradient of optimal torque) whereas the st-MPC ignores the dynamics and hence the st-MPC's optimal control input and torque trajectories are exactly the same, iii) the bottom figure in Fig. 3(b) shows the output trajectory (also referred as 'measured' or 'actual' trajectory in this paper), i.e., the trajectory realised by the ICE plant model when excited with the control inputs from both the controllers, from which it could be observed that the plant output follows the predicted optimal torque trajectory in case of dy-MPC perfectly whereas it lags in case of the st-MPC (w.r.t. its prediction) due to the model dynamics mismatch, as expected.

Since the ISG dynamics (relatively smaller w.r.t. the ICE dynamics) were ignored by both the controllers, the predicted and the plant output torque trajectories were exactly same for each controller, i.e., no difference between the st-MPC (or dy-MPC) prediction and the plant output when excited with the control from the st-MPC (or dy-MPC), but the trajectories of both the controllers deviate from each other corresponding to the deviation of their optimal ICE torque trajectories. These deviations affect the energy consumption trajectories and are explained in V-B2.

2) Effect of Actuator Dynamics on Energy Consumption: Figure 4 shows the comparison of the prediction versus measured cost trajectories for both the controllers at $\tau_{\text{ice}} = 1\,\text{s}$. i) From the fuel cost trajectories (top figure) shown in Fig. 4, it could be noted that in case of st-MPC, the deviation of the measured fuel cost w.r.t. the predicted trajectory increases with time due to the accumulation of errors introduced by the absence of an ICE dynamic model in st-MPC, whereas in case of dy-MPC, both the measured and the predicted fuel cost

trajectories match exactly, since they share the same dynamic ICE model. Due to this, the st-MPC consumes 4.5% (deviation of measured costs) more fuel energy w.r.t. the dy-MPC inspite of a deviation of just 0.22% among their predicted costs. The reason for the difference between the deviations in fuel costs is that the lower-level controller compensates the fuel supplied to the ICE corresponding to the vehicle speed error feedback (as explained in V-A), introduced by the ICE dynamics mismatch in case of the st-MPC whereas there's no such effect in the dy-MPC since its speed error is zero. ii) the battery SOE trajectory (bottom figure) of both the controllers shown in Fig. 4, closely match each other since they use the same static model of ISG. But due to the ICE dynamics mismatch, the st-MPC charges the battery to 0.08% higher SOE (deviation of measured costs) w.r.t. the dy-MPC (unlike the increase in st-MPC's fuel consumption) whereas the predicted deviation was just an increase of 0.03% of battery SOE. Again, the increase in battery SOE measured, w.r.t. prediction, is because the lower level controller uses the ISG to recover some part of the excess energy supplied by ICE (remaining energy is lost in friction brakes) due to dynamics mismatch, in case of the st-MPC. iii) Hence, the controller with the proposed optimal power-split strategy, dy-MPC, was able to achieve a total energy saving of 4.25% w.r.t. st-MPC in the WLTC Class-3b drive cycle, as an increase of 0.08% of battery SOE corresponds to a 0.25% change in cumulative fuel energy consumption.

C. Performance of Proposed Strategy w.r.t. Driving Missions

To evaluate the performance of the dy-MPC (with $\tau_{\mathrm{ice}} = 1\,\mathrm{s}$) under different driving scenarios like different levels of maximum speed, maximum acceleration, and aggressive driving behaviours, Common Artemis Driving Cycles (CADC) and US06 - Supplemental Federal Test Procedure (US06-SFTP) are used in addition to the WLTC Class-3b cycle. The different vehicle demands of these driving missions and the corresponding energy savings ($\%$) achieved by the dy-MPC w.r.t. st-MPC, are listed in Table I.

From the results, it is clear that i) the combined effect of higher speeds, acceleration and no. of acceleration instances (i.e., the regions where the powertrain experiences the effect of ICE dynamics) in the CADC-Rural road cycle enables the dy-MPC to achieves a maximum energy savings of 10.95%, ii) the energy savings achieved in US06 cycle is lesser than the CADC-Rural Road due to its lower instances of acceleration (inspite of boosting a higher max. speed and $a_{\max}$ requirements) whereas in comparison to the WLTC cycle, the energy savings in US06 are more (inspite of lower instances of acceleration) due to the higher acceleration demand, iii) Among the CADC cycles (since their $a_{\max}$ is the same) the dy-MPC achieves a lower energy saving of 6.74% in Motorway cycle due to lower no. of acceleration region whereas it achieves a medium and the highest energy savings in the Urban (7.27%) and the Rural road (10.95%) cycles, respectively, due to the difference in their maximum (and average) speed demand, iv) the least energy savings is achieved in WLTC cycle due to the least $a_{\max}$ and a lower acceleration instances. Another important aspect of the drive cycles that played a major part in the achieved results, apart from the transient factors shown in the Table I, is the percentage duration of these transient factors being active (non-zero) in relation to the total duration of the drive cycle. These results show that the energy saving ($\%$) potential of the dy-MPC depends majorly on the factors like maximum (and average) speed, maximum acceleration, the available number of acceleration instances, and the active (non-zero) duration of these transient factors in the complete drive cycle. i.e., the maximum energy saving potential of the proposed strategy depends on the severity of the transient load demand in the driving mission.

TABLE I
PERFORMANCE OF THE PROPOSED STRATEGY W.R.T. DRIVE CYCLES

Drive Cycle	Max. Speed [kmph]	Max. Acc. (a_max) [m/s^2]	No. of Acc.'s	Total Distance [km]	Energy Savings [%]
WLTC (Class 3b)	131.30	1.58	31	23.27	4.25
CADC (Urban)	57.32	2.44	48	4.87	7.27
CADC (Rural Road)	111.09	2.44	48	17.28	10.96
CADC (Motorway)	150.37	2.44	43	29.55	6.74
US06-SFTP	128.91	3.8	20	12.89	8.94

D. Sensitivity of Energy Savings w.r.t. Actuator Dynamics

In the considered HEV powertrain, different potential ICE configurations (specifically tuned for high power/weight ratio, performance vs fuel efficiency, and component cost reduction) could be realised by configuring systems like supercharging and turbocharging accordingly [9], [22], [23]. But these mechanisms affect the ICE dynamics differently; like the turbocharger, which is mostly tuned to operate in medium and high speed regions of the ICE, induces lag in torque delivery whereas a supercharger, usually operates in the low and medium speed regions, improves the ICE torque response [22], [23]. Hence, when the operating speed of the ICE crosses between the active and inactive regions of these mechanisms, and during load changes, it experiences rapid fluctuations due to torque ripples resulting in a 'Jerk' of the crankshaft [26]. To overcome this problem, the rate of change of the torque delivered is controlled, called Anti-Jerk control, by the lower-level controller of the ICE such that the engine acceleration is smoother but this results in additional losses and hence, consumes additional fuel. So, this functionality is calibrated to achieve a desired ICE dynamic behaviour against its consumption, based on the specification of the ICE configuration and its performance requirements. Hence, to evaluate the energy saving potential of the proposed power-split strategy within the allowable tuning values of the ICE dynamic behaviour in the considered HEV powertrain, a sensitivity analysis is performed by varying the dynamic torque model parameter, τ_{ice}, of both the simulation plant and the dy-MPC controller

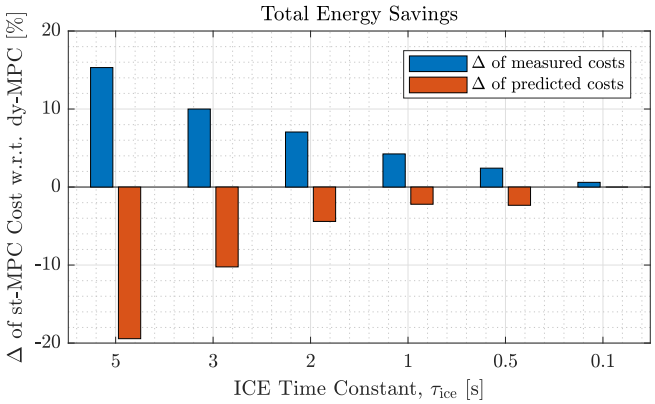

Fig. 5. Percentage variation in the total energy consumption (arithmetic sum of variations of the cumulative fuel and battery energy consumption) of the st-MPC w.r.t dy-MPC under different levels of ICE dynamic response tuning. The result shows that the dy-MPC can maximise energy savings when the actuator dynamics are increasing sluggish in nature, for the considered HEV powertrain configuration.

models simultaneously, to values of $0.1\,\text{s}, 0.5\,\text{s}, 1\,\text{s}, 2\,\text{s}, 3\,\text{s}$, and $5\,\text{s}$, to represent each tuning scenario.

i) The Fig. 5 shows the total energy savings (blue bar graph) achieved by the proposed strategy in WLTC Class-3b drive cycle, from which it could observed that the deviation of total cost (energy consumption) measurement of the st-MPC w.r.t the dy-MPC (Δ of measured costs), exhibits a polynomial increase as the value of τ_{ice} becomes larger, which shows that the st-MPC struggles severely with a non-optimal control policy whereas the dy-MPC realises a polynomial increase in energy savings, as the τ_{ice} increases. ii) From Δ of predicted costs in the red coloured bar graph in Fig. 5, i.e., the deviation of the total energy consumption predicted by the st-MPC w.r.t. the prediction of dy-MPC, it could be noted that the st-MPC had predicted a lower energy consumption understandably, as it hadn't considered the additional limitation of dynamics and hence, had chosen a more efficient but an unrealizable power-split trajectory. iii) These results show that the dy-MPC becomes a better choice for the considered HEV powertrain (assuming that the computational system is able to accommodate an additional load of $< 35\%$ within each control interval), when the torque response of the chosen ICE configuration is sluggish whereas the st-MPC could be a better option for $\tau_{\text{ice}} < 0.1\,\text{s}$, as the energy savings achieved by the dy-MPC for $\tau_{\text{ice}} < 0.1\,\text{s}$ are meagre for the additional computational load it demands.

In other words, it can be stated that the anti-Jerk control functionality, in a HEV powertrain equipped with the dy-MPC for optimal power-split, could be tuned such that the ICE dynamic response is as sluggish as allowed by its performance criteria (under the assumption that the battery SOE stays within its limits during the driving mission), to achieve maximum energy savings as well as a smoother ICE acceleration, the two conflicting performance parameters in ICE control otherwise.

VI. Conclusion

In this paper, the control-oriented models of a gasoline ICE torque dynamics and its fuel consumption dynamics has been proposed and experimentally validated. Then, an MPC based supervisory control strategy, which incorporates the proposed dynamic models explicitly in the power-split controller for minimising the fuel and energy consumption in HEVs has been proposed. The performance of the proposed strategy has been validated in a parallel HEV platform against a base power-split controller (without ICE dynamic models) for comparison. Our results show that the proposed optimal power-split control strategy, which incorporates ICE dynamic models, is able to realise higher fuel and equivalent energy savings w.r.t the base controller in a drive cycle where the transient load demands are present. Also, the evaluation of the proposed strategy under different driving scenarios shows that the control strategy realises maximum energy savings depending on the severity of the transient load demands in a driving mission. Further analysis of the actuator's dynamic model parameter variation shows that the proposed control strategy achieves considerable energy savings when the powertrain actuator dynamics (or) responses are slower. These results portray the significance of considering the actuator dynamics explicitly in the optimal power-split controllers for HEVs, especially when the actuators have (or) are dynamically controlled to have a sluggish response and the driving mission has considerable transient load demands.

Acknowledgment

The authors would like to thank the Sweden´s Innovation Agency (Vinnova), the Volvo Car Corporation and the Chalmers University of Technology for their support.

References

[1] A. Sciarretta, M. Back, and L. Guzzella, "Optimal control of parallel hybrid electric vehicles," *IEEE Transactions on Control Systems Technology*, vol. 12, pp. 352–363, May 2004. Conference Name: IEEE Transactions on Control Systems Technology.

[2] P. Pisu and G. Rizzoni, "A Comparative Study Of Supervisory Control Strategies for Hybrid Electric Vehicles," *IEEE Transactions on Control Systems Technology*, vol. 15, pp. 506–518, May 2007.

[3] A. Sciarretta and L. Guzzella, "Control of hybrid electric vehicles," *IEEE Control Systems Magazine*, vol. 27, pp. 60–70, Apr. 2007.

[4] N. Murgovski, L. Johannesson, J. Hellgren, B. Egardt, and J. Sjöberg, "Convex Optimization of Charging Infrastructure Design and Component Sizing of a Plug-in Series HEV Powertrain," *IFAC Proceedings Volumes*, vol. 44, pp. 13052–13057, Jan. 2011.

[5] N. Murgovski, L. Johannesson, J. Sjöberg, and B. Egardt, "Component sizing of a plug-in hybrid electric powertrain via convex optimization," *Mechatronics*, vol. 22, pp. 106–120, Feb. 2012.

[6] G. Liu and J. Zhang, "Comparative Study of Optimal Control Strategies for the Range-extended Electric Vehicle," *DEStech Transactions on Engineering and Technology Research*, vol. 0, no. ICMITE2016, 2016.

[7] M. Montazeri-Gh, Z. Pourbafarani, and M. Mahmoodi-k, "Comparative study of different types of PHEV optimal control strategies in real-world conditions," *Proceedings of the Institution of Mechanical Engineers, Part D: Journal of Automobile Engineering*, vol. 232, pp. 1597–1610, Oct. 2018. Publisher: IMECHE.

[8] IEA, "Global EV Outlook 2019," tech. rep., IEA, Paris, 2019. www.iea.org.

[9] L. Guzzella and A. Sciarretta, *Vehicle Propulsion Systems*. Berlin, Heidelberg: Springer-Verlag Berlin Heidelberg, 3 ed., 2013.

[10] T. Hofman, M. Steinbuch, R. M. van Druten, and A. F. A. Serrarens, "Rule-Based Energy Management Strategies for Hybrid Vehicle Drivetrains: A Fundamental Approach in Reducing Computation Time," *IFAC Proceedings Volumes*, vol. 39, pp. 740–745, Jan. 2006.

[11] R. Biasini, S. Onori, and G. Rizzoni, "A near-optimal rule-based energy management strategy for medium duty hybrid truck," *International Journal of Powertrains*, vol. 2, no. 2/3, pp. 232–261, 2013.

[12] N. Schouten, M. Salman, and N. Kheir, "Fuzzy logic control for parallel hybrid vehicles," *IEEE Transactions on Control Systems Technology*, vol. 10, pp. 460–468, May 2002.

[13] F. Khoucha, M. Benbouzid, and A. Kheloui, "An optimal fuzzy logic power sharing strategy for Parallel Hybrid Electric Vehicles," (Lille, France), pp. 1–5, IEEE, Sept. 2010. ISSN: 1938-8756.

[14] J. Wu, C. H. Zhang, and N. X. Cui, "Fuzzy energy management strategy for a hybrid electric vehicle based on driving cycle recognition," *International Journal of Automotive Technology*, vol. 13, pp. 1159–1167, Dec. 2012.

[15] C. H. Zheng, G. Q. Xu, S. W. Cha, and Q. Liang, "Numerical comparison of ECMS and PMP-based optimal control strategy in hybrid vehicles," *International Journal of Automotive Technology*, vol. 15, pp. 1189–1196, Dec. 2014.

[16] Y. Zou, H. Shi-jie, L. Dong-ge, G. Wei, and X.-s. Hu, "Optimal Energy Control Strategy Design for a Hybrid Electric Vehicle," *Discrete Dynamics in Nature and Society*, vol. 2013, p. 8 pages, Feb. 2013.

[17] F. Zhang, K. Xu, C. Zhou, S. Han, H. Pang, and Y. Cui, "Predictive Equivalent Consumption Minimization Strategy for Hybrid Electric Vehicles," in *2019 IEEE Vehicle Power and Propulsion Conference (VPPC)*, pp. 1–5, Oct. 2019. ISSN: 1938-8756.

[18] N. Kim, S. Cha, and H. Peng, "Optimal Control of Hybrid Electric Vehicles Based on Pontryagin's Minimum Principle," *IEEE Transactions on Control Systems Technology*, vol. 19, pp. 1279–1287, Sept. 2011.

[19] F. Yan, J. Wang, and K. Huang, "Hybrid Electric Vehicle Model Predictive Control Torque-Split Strategy Incorporating Engine Transient Characteristics," *IEEE Transactions on Vehicular Technology*, vol. 61, pp. 2458–2467, July 2012.

[20] M. Bidarvatan and M. Shahbakhti, "Impact of Engine Dynamics on Torque Split Management of a Hybrid Electric Vehicle," (San Antonio, Texas, USA), p. 10, Dec. 2014.

[21] M. Bidarvatan and M. Shahbakhti, "Analysis and Control of Torque Split in Hybrid Electric Vehicles by Incorporating Powertrain Dynamics," *Journal of Dynamic Systems, Measurement, and Control*, vol. 140, Nov. 2018.

[22] L. Guzzella and C. H. Onder, *Introduction to Modeling and Control of Internal Combustion Engine Systems*. Berlin, Heidelberg: Springer, 2010.

[23] R. Isermann, *Engine Modeling and Control: Modeling and Electronic Management of Internal Combustion Engines*. Berlin Heidelberg: Springer-Verlag, 2014.

[24] C. J. Oglieve, M. Mohammadpour, and H. Rahnejat, "Optimisation of the vehicle transmission and the gear-shifting strategy for the minimum fuel consumption and the minimum nitrogen oxide emissions," *Proceedings of the Institution of Mechanical Engineers, Part D: Journal of Automobile Engineering*, vol. 231, pp. 883–899, June 2017.

[25] S. Onori, L. Serrao, and G. Rizzoni, *Hybrid Electric Vehicles: Energy Management Strategies*. No. 2192-6786 in SpringerBriefs in Control, Automation and Robotics, London: Springer-Verlag, 1 ed., 2016.

[26] T. Pham, R. Seifried, and C. Scholz, "Anti-Jerk Control of a Parallel Hybrid Electrified Vehicle with Dead Time," *IFAC-PapersOnLine*, vol. 50, pp. 966–971, July 2017.